*Article*

# Chirality and Relativistic Effects in Os$_3$(CO)$_{12}$

**Maxim R. Ryzhikov** [ID]**, Irina V. Mirzaeva** [ID]**, Svetlana G. Kozlova** [ID] **and Yuri V. Mironov \*** [ID]

Nikolaev Institute of Inorganic Chemistry SB RAS, 3, Acad. Lavrentiev Ave., 630090 Novosibirsk, Russia; maximato@mail.ru (M.R.R.); dairdre@gmail.com (I.V.M.); sgk@niic.nsc.ru (S.G.K.)

\* Correspondence: yuri@niic.nsc.ru

**Abstract:** The energy and structural parameters were obtained for all forms of the carbonyl complex of osmium Os$_3$(CO)$_{12}$ with D$_{3h}$ and D$_3$ symmetries using density functional theory (DFT) methods. The calculations took into account various levels of relativistic effects, including those associated with nonconservation of spatial parity. It was shown that the ground state of Os$_3$(CO)$_{12}$ corresponds to the D$_3$ symmetry and thus may be characterized either as left-twisted (D$_{3S}$) or right-twisted (D$_{3R}$). The D$_{3S} \leftrightarrow$D$_{3R}$ transitions occur through the D$_{3h}$ transition state with an activation barrier of ~$10^{-14}$ kJ/mol. Parity violation energy difference (PVED) between D$_{3S}$ and D$_{3R}$ states equals to ~$5 \times 10^{-10}$ kJ/mol. An unusual three-center exchange interaction was found inside the {Os$_3$} fragment. It was found that the cooperative effects of the mutual influence of osmium atoms suppress the chirality of the electron system in the cluster.

**Keywords:** structure of the Os$_3$(CO)$_{12}$ clusters; chirality; relativistic effects; parity violating energy difference; quantum chemistry

check for **updates**

## 1. Introduction

It is well known that enantiomerism is directly related to the origin of life on Earth. Many essential biological and chemical processes are stereoselective, involving only one enantiomer, which exists independently from its chiral counterpart. Separation of one enantiomer from another is not only important for practical use, but also sparks much interest as a fundamental problem, which constantly attracts research attention to the spatial and electronic structure of enantiomers [1–3]. In particular, especially interesting is how the parity violating weak nuclear forces may manifest in chiral molecules and may be somehow responsible for the choice of which enantiomer would prevail in living organisms [4–7].

Molecules with D$_3$ symmetry are particularly interesting because they are characterized either with left-handed (D$_{3S}$) or with right-handed (D$_{3R}$) torsion, which allows these structures to be treated as chiral enantiomers. Previously, the detailed analysis of the 1,4-diazabicyclo[2.2.2]octane (DABCO) molecule with D$_{3S}$ (left-twisted), D$_{3R}$ (right-twisted), and D$_{3h}$ (untwisted) symmetries in gas phase and in Metal-organic Frameworks (MOFs) was performed [8,9]. There were expectations that MOFs with a DABCO linker may undergo a number of phase transitions related to enantiomers ordering [2,10], and that cooperative effects in such systems may help the experimental search of molecular parity violation effects [7,9,11]. However, the energy barrier between the D$_{3S}$ and D$_{3R}$ states of DABCO appears to be very low (<100 J/mol in gas phase [8] and ~5 kJ/mol in MOF [9]), which makes MOFs with DABCO difficult for experimental studies of such effects.

Similarly to the DABCO molecule, trinuclear transition metal cluster complexes may also have D$_3$ symmetry. A well-known carbonyl osmium complex Os$_3$(CO)$_{12}$ (Figure 1) is widely used in synthesis in organometallic and inorganic chemistry [12–14]. It acts as a catalyst for a wide range of reactions [15]. It was considered as a model system for studies of mechanisms of photoinduced reactions [16–18] and vibrational and NMR spectroscopy [19–21]. In crystal, which is reported to have a monoclinic space group P2$_1$/n,

the $Os_3(CO)_{12}$ molecules show approximate (pseudo-) $D_{3h}$ symmetry, where the three Os atoms form an almost equilateral triangle [22]. Previous detailed quantum chemical studies of structure and interatomic interactions in the $Os_3(CO)_{12}$ cluster have shown that in the gas phase, the ground state has the $D_3$ symmetry, while the $D_{3h}$ symmetry refers to a transition state. It was also found that there is another transition state with $C_{2v}$ symmetry and higher energy, which, however, may occur at high temperatures [23–25].
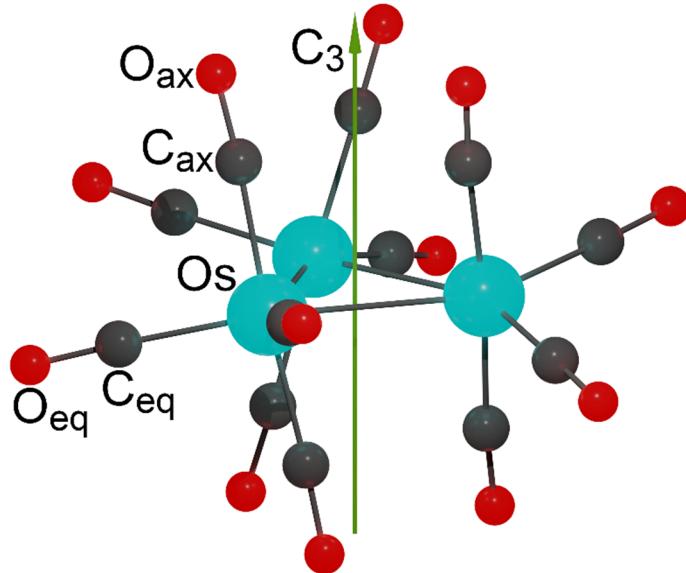


**Figure 1.** The structure of $Os_3(CO)_{12}$ cluster corresponding to the local minimum on PES.

In the present study, for the first time, the $Os_3(CO)_{12}$ cluster was considered as a chiral compound. We investigated what exactly is responsible for the stabilization of the twisted $D_3$ structure compared to the untwisted $D_{3h}$ one. We also evaluated the impact of relativistic effects on the structure and energetics of the $Os_3(CO)_{12}$ clusters, including the parity violation energy shift due to the weak nuclear forces. We expected that due to the cooperative effects, such trinuclear transition metal clusters may become a good family of systems for the experimental molecular parity violation search.

## 2. Results and Discussion

### 2.1. Structure and Energetics of $Os_3(CO)_{12}$

The analysis of the interatomic distances in $Os_3(CO)_{12}$ (Table 1 and Table S1) shows that the best agreement between calculated and experimental X-ray diffraction (XRD) structures [22,26] was observed for the calculations with relativistic effects. Moreover, the difference between scalar (SR) and spin–orbit (SO) relativistic methods is rather small. However, they both are very different from the nonrelativistic (NR) level of theory. In this case, the $D_{3h}$ is the local minimum without imaginary frequencies in vibrational spectrum, while the $D_3$ symmetry refers to just some point on potential energy surface (PES) and is characterized with two imaginary frequencies. The energy difference between the structures with $D_3$ and $D_{3h}$ symmetries calculated at the relativistic level (SR and SO) indicates that the $D_3$ state is the local minimum on the potential energy surface. At both SR and SO levels of theory, there are no imaginary frequencies for the structure with $D_3$ symmetry, while $D_{3h}$ is a transition state with a single imaginary frequency. Gibbs free energy differences between $D_3$ and $D_{3h}$ structures are 13.8 kJ/mol and 10.5 kJ/mol for SR and SO levels of theory, respectively (Figure 2). Previous calculations with relativistic effective core potential (ECP) also indicated that the $D_3$ state is a local minimum [25]. Thus, it can be concluded that the $D_3$ is the local minimum in the gas phase and the taking into account the relativistic effects at least at ECP level is necessary for correct description of the system.

**Table 1.** Interatomic distances (Å), dihedral angles (°), energy differences (kJ/mol), and number of imaginary frequencies (n$i$) for $Os_3(CO)_{12}$ clusters with $D_3$ and $D_{3h}$ symmetries. Error estimates shown in parentheses for average ($<x>$) distances or angles are the exterior estimates of the precision of the average value given by $[\Sigma(<x> - x)^2/(m^2 - m)]^{1/2}$ (m is the number of x values) [22]. The TPSSh + D4(EEQ)/TZ2P and MPW1PW91/SDD are the theoretical levels used for geometry optimization (for details see Section 3). NR, SR, SO and ECP are the relativistic levels used in quantum chemical calculations. The average experimental distances and angles were taken from X-ray diffraction (XRD) data [22,26].

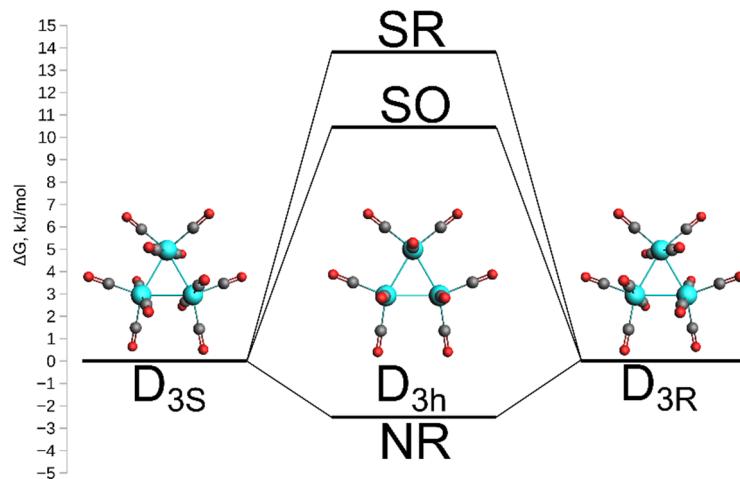| | TPSSh + D4(EEQ)/ TZ2P | | | TPSSh + D4(EEQ)/ TZ2P | | | XRD [22] | XRD [26] | MPW1PW91 /SDD [25] | |
|---|---|---|---|---|---|---|---|---|---|---|
| Symmetry | $D_3$ | | | $D_{3h}$ | | | Pseudo-$D_{3h}$ | Pseudo-$D_{3h}$ | $D_3$ | $D_{3h}$ |
| Relativity level | NR | SR | SO | NR | SR | SO | | | ECP | ECP |
| d(Os-Os) | 2.808 | 2.869 | 2.869 | 2.801 | 2.883 | 2.884 | <2.877>(3) | <2.881>(4) | 2.895 | 2.907 |
| d(Os-C$_{eq}$) | 1.968 | 1.916 | 1.914 | 1.966 | 1.915 | 1.914 | <1.912>(7) | <1.919>(36) | 1.917 | 1.917 |
| d(Os-C$_{ax}$) | 2.001 | 2.11 | 1.955 | 1.992 | 1.954 | 1.953 | <1.946>(6) | <1.973>(12) | 1.953 | 1.95 |
| ∠C-Os-Os-C | 37.2 | 29.3 | 29.2 | 0 | 0 | 0 | <2.1>(5) | <1.3>(1.3) | 31.4 | 0 |
| ∠C$_{3axes}$-Os-C | 21.2 | 16.8 | 16.8 | 0 | 0 | 0 | <1.2>(5) | <0.7>(1.0) | 18 | 0 |
| ΔE | 0 | 0 | 0 | −3.0 | 7.5 | 7.7 | - | - | −2.3 | 0 |
| ΔG | 0 | 0 | 0 | −2.5 | 13.8 | 10.5 | - | - | - | - |
| n$i$ | 2 | 0 | 0 | 0 | 1 | 1 | - | - | 0 | 1 |



**Figure 2.** The barrier height for the $D_{3S} \leftrightarrow D_{3R}$ enantiomerization through the $D_{3h}$ transition state calculated at nonrelativistic (NR), scalar (SR) and spin-orbit (SO) relativistic levels of theory.

The main difference between experimental XRD data and relativistic calculations (for both SR and SO methods) is found in the dihedral angles ∠C-Os-Os-C и∠C$_{3axes}$-Os-C, which characterize the degree of the twisting of the $Os_3(CO)_{12}$ structure. Such a difference could be related to the packing effects in the solid state. In order to compare the packing energy with the barrier between the cluster structures with $D_{3S}$ and $D_{3R}$ symmetries, the periodic calculations were performed. The packing energy is ~ 44 kJ/mol per cluster, while the barrier is ~10 kJ/mol. Thus, the packing effect is big enough to suppress the twisting of the $Os_3(CO)_{12}$ clusters in the solid state.

The energy difference between $D_3$ and $D_{3h}$ structures characterizes the barrier between $D_{3S}$ and $D_{3R}$ enantiomers of $Os_3(CO)_{12}$ cluster. Without consideration of parity violating interactions, $D_{3S}$ and $D_{3R}$ enantiomers have exactly the same energy and electronic structure. The geometries of $D_{3S}$ and $D_{3R}$ enantiomers differ only by the sign of the Z coordinates of the atoms (Table S1). Thus, any of the enantiomers can be used to analyze the interactions in the cluster.

The barrier between $D_{3S}$ and $D_{3R}$ is low (~10–14 kJ/mol). Thus, similarly to the DABCO molecule [1], at room temperature there should be a dynamical equilibrium between $D_{3S}$ and $D_{3R}$ structures resulting in a quasi-$D_{3h}$ structure.

## 2.2. Characterization of the Interactions in the $Os_3(CO)_{12}$ Cluster

The energy decomposition analysis (EDA) of the interactions between $Os(CO)_4$ fragments in the $Os_3(CO)_{12}$ cluster show that the orbital interactions' contributions to stabilization of the $D_3$ structure are larger than for the $D_{3h}$ form (Table 2). On the contrary, the steric interactions destabilize $D_3$ compared to the $D_{3h}$. The distortions of the $Os(CO)_4$ fragments in the clusters, as well as dispersion interactions, have only minor impacts on the energy difference between structures with $D_3$ and $D_{3h}$ symmetries and, in general, compensate each other. Thus, the stronger orbital interactions between the $Os(CO)_4$ fragments are the main factors that are responsible for the stability of the $D_3$ form.

**Table 2.** Results of energy decomposition analysis (EDA) for interactions between $Os(CO)_4$ fragments in $D_3$ and $D_{3h}$ forms of $Os_3(CO)_{12}$ calculated at TPSSh + D4(EEQ) + SR/QZ4P//TPSSh + D4(EEQ) + SR/TZ2P level of theory. The formation energies of the fragments ($E_{frag}(Os(CO)_4$) as well as energies of steric ($E_{Steric}$), orbital ($E_{Orbital}$), dispersion ($E_{Disp}$) and total ($E_{Int}$) interactions between fragments are given in kJ/mol.

| | $E_{frag}(Os(CO)_4)$ | $E_{Steric}$ | $E_{Orbital}$ | $E_{Disp}$ | $E_{Int}$ |
|---|---|---|---|---|---|
| $D_3$ | −7838.3 | 520.1 | −1191.6 | −118.4 | −789.9 |
| $D_{3h}$ | −7839.6 | 489.5 | −1153.1 | −114.2 | −778.2 |
| $\Delta(D_3-D_{3h})$ | 1.3 | 30.5 | −38.5 | −4.2 | −11.7 |

ELF analysis of the interactions in the osmium triangle showed the presence of the three valence V(Os, Os) basins (Figure 3), which indicate the covalency of the interactions between Os atoms in both $D_3$ and $D_{3h}$ structures of $Os_3(CO)_{12}$ cluster. Also, both structures are characterized with the single trisynaptic basin in the center of $Os_3$ triangle. However, this basin does not have common borders with any of the core basins (Figures S1 and S2). It shares borders only with valence V(Os, Os) basins and, thus, this basin indicates the electron exchange between V(Os, Os) basins. To our best knowledge, it is the first example of such ELF topology. Formally, this basin should be classified as V(V(Os, Os)$_3$). In the list of the molecular orbitals, the HOMO-2 (Figure 4) could be the one responsible for this V(V(Os, Os)$_3$) basin. Note that the populations of the V(V(Os, Os)$_3$) basins are very small (0.03e and 0.01e for $D_3$ and $D_{3h}$ structures, respectively), however it should provide the exchange between V(Os, Os). This assumption is consistent with results of previous QTAIM analysis about three center interactions in $Os_3(CO)_{12}$ cluster [23].

## 2.3. Chirality and Parity Violation in $Os_3(CO)_{12}$

Our calculations indicate that relativistic effects define the $D_3$ symmetry of the ground state of $Os_3(CO)_{12}$ molecule, which has the two variants: left-twisted $D_{3S}$ and right-twisted $D_{3R}$. The next level of relativistic effects would be the calculation of the contributions of the nuclear weak forces to the energy of the system. These forces violate spatial parity symmetry; thus, they make the energy of enantiomers slightly different. Experimental evidence of such effect have been observed on nuclear and atomic levels [27]. However, parity violation effects on molecular level have not been detected experimentally yet [7]. Thus, it is important to look for good candidates for experimental search of molecular parity violation.

The major contribution to PVED comes from the nuclear-spin-independent part of the parity-violating Hamiltonian [28]:

$$H_{PV}^{SI} = \frac{G_F}{2\sqrt{2}} \sum_{m}^{N_{nuc}} \left( Q_W(n) \gamma^5 \rho_n(r) \right),\tag{1}$$

where $G_F$ is the Fermi-coupling constant with a value of $2.22255 \times 10^{-14}$ a.u.; $\gamma^5$ is the fifth Dirac gamma matrix, which refers to the electron chirality operator; $\rho_n(r)$ is the normalized nucleon density; $N_{nuc}$ is the number of nuclei in the molecule; and $Q_W(n)$ is the weak

nuclear charge of nucleus $n$, which depends on the number of protons $Z(n)$ and neutrons $N(n)$ in the nucleus. It is given by the expression:

$$Q_W(n) = Z(n)\left(1 - 4\sin^2\theta_W\right) - N(n) \qquad (2)$$
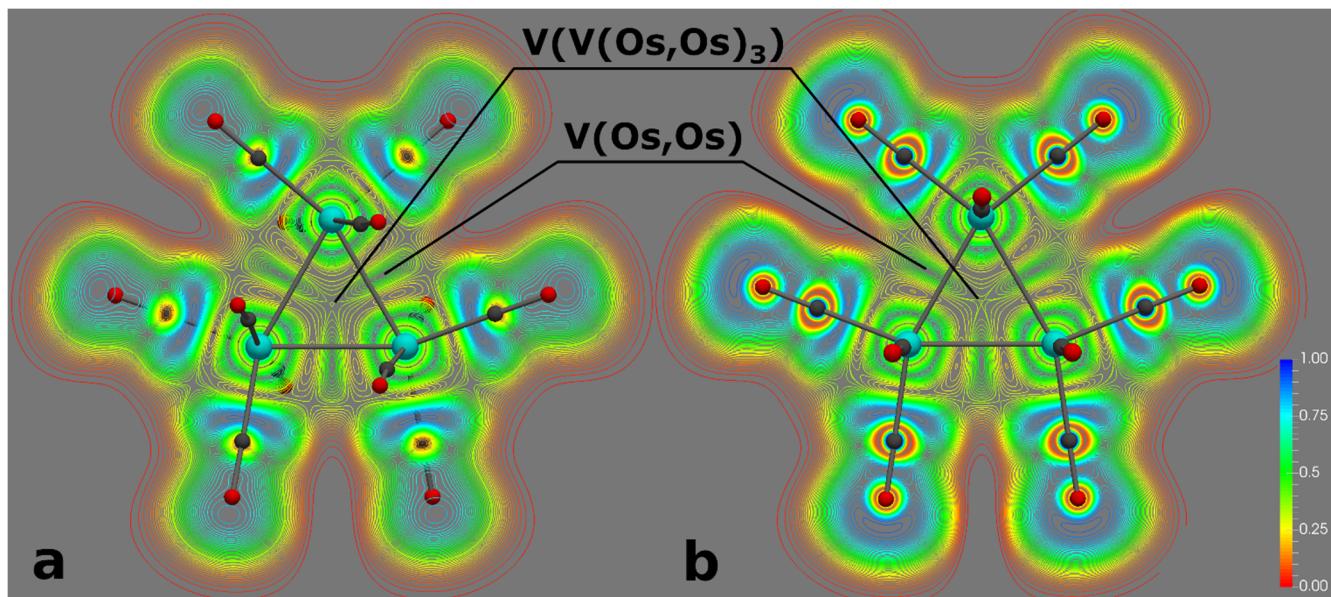
with $\theta_W$ being the Weinberg angle.



**Figure 3.** ELF slice planes for $Os_3(CO)_{12}$ clusters with $D_3$ (**a**) and $D_{3h}$ (**b**) symmetries.
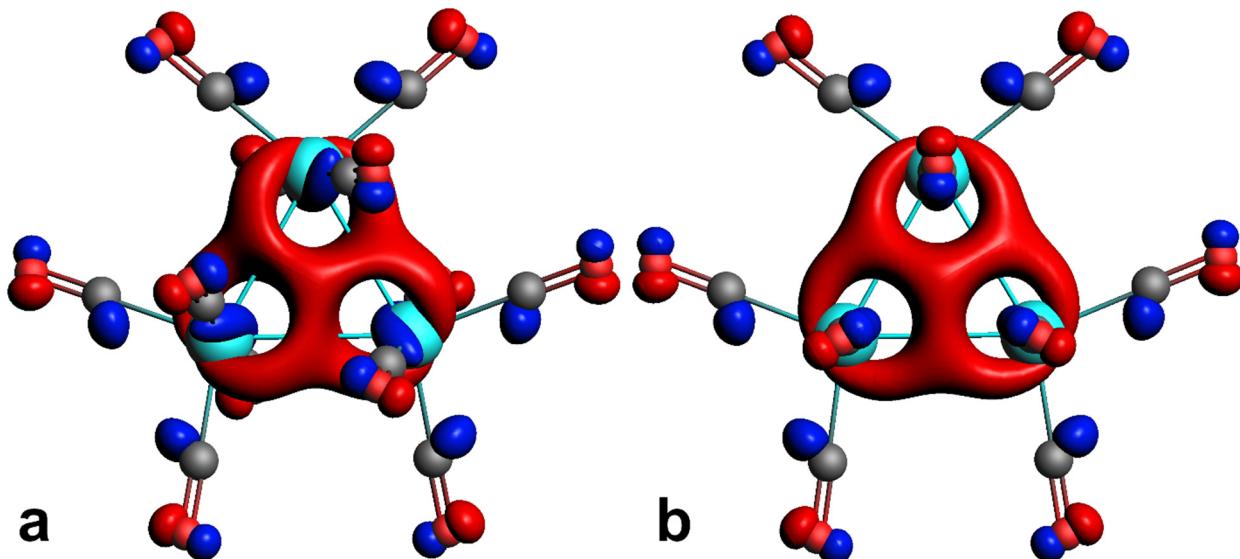


**Figure 4.** HOMO-2 orbitals for $Os_3(CO)_{12}$ clusters with $D_3$ (**a**) and $D_{3h}$ (**b**) symmetries.

Previous Density Functional Theory (DFT), Hartree-Fock method (HF), and Many Body Perturbation Theory (MBPT) calculations for compounds of various six-row elements showed rather low values of PVED: ~$3 \times 10^{-12}$ kJ/mol for Hg [9], ~$6 \times 10^{-11}$ kJ/mol for Re and ~$2 \times 10^{-10}$ for Os [29], up to ~$2 \times 10^{-10}$ for Bi [30], and the largest would be ~$8 \times 10^{-9}$ kJ/mol for the hypothetical analogue of hydrogen peroxide—$Po_2H_2$ [31]. However, some of those estimations were made using approximate two-component relativistic methods, while our previous work showed that results of two-component PVED

calculations in some systems may differ from the four-component results by up to 30% [11]. Therefore, in this work we used only fully relativistic four-component methods for calculations of PVED.

We may try to estimate the characteristic PVED values for Os compounds. As weak interactions are local and largely depend on the atomic number, the main contribution would be from the heaviest nucleus in the molecule (in our case Os) and may be estimated as follows [32]:

$$PVED \approx G_F \alpha^3 Z^4 N K_r \eta \tag{3}$$

where $\alpha$ is the fine-structure constant, $Z$ is the charge of the heaviest nucleus in the molecule, $N$ is the number of neutrons in the heaviest nucleus in the molecule, $K_r$ is some enhancement factor for relativistic effects (for the first row atoms $K_r \sim 1$, while for the heavier period six elements $K_r \sim 10$), and $\eta$ is the dimensionless molecular asymmetry factor. The estimations of typical $\eta$ in organic molecules fall in the range from $\sim 10^{-9}$ [33] to $\sim 10^{-2}$ [34]. Therefore, according to Equation (3), PVED in Os compounds may be preliminarily estimated as $\sim 8 \times 10^{-16}$–$\sim 8 \times 10^{-9}$ kJ/mol.

Especially interesting are the possible cooperative effects in trinuclear $Os_3(CO)_{12}$ clusters. The contributions from the three Os atoms may just sum up, but also it may either additionally increase or suppress the chirality of the system. To extract such effects, we may compare the PVED values for $Os_3(CO)_{12}$ with some mononuclear reference system. We chose the hypothetical OsOSSeTe complex, which is analogous to the osmium tetraoxide. The results are shown in Table 3. The PVED values for $Os_3(CO)_{12}$ are closer to the upper estimate for Os compounds. We can see that Generalized Gradient Approximation (GGA) methods consistently give lesser values than HF, while hybrid and range-separated methods predictably give half-way values. This is supported by the electron chirality density pictures (Figure 5). The most surprising is the strong dependence of PVED for OsOSSeTe from the method used. This is due to the fact that contribution from the second heavy atom Te is of the opposite sign and DFT GGA methods, for some reason, redistribute the electron chirality in such a way that it becomes much higher on the Te atom. However, even the largest PVED value for OsOSSeTe (HF) is an order of magnitude less than the corresponding value for $Os_3(CO)_{12}$.

**Table 3.** PVED (kJ/mol) calculated with different methods: Hartree-Fock (HF) and DFT with functionals PBE [35], PBE0 [36], BLYP [37], B3LYP [38], CAMB3LYP [39].

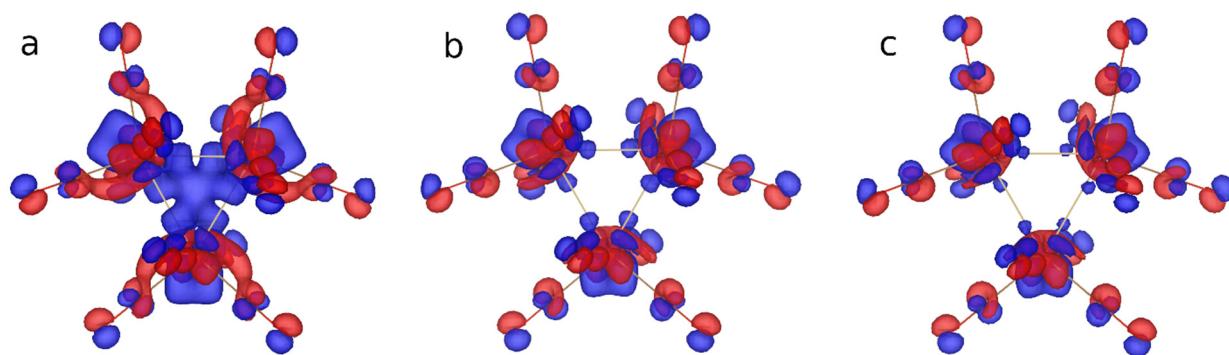| | HF | PBE | PBE0 | BLYP | B3LYP | CAMB3LYP |
|---|---|---|---|---|---|---|
| $Os_3(CO)_{12}$ | $6.66 \times 10^{-10}$ | $3.87 \times 10^{-10}$ | $4.61 \times 10^{-10}$ | $4.14 \times 10^{-10}$ | $4.77 \times 10^{-10}$ | $5.51 \times 10^{-10}$ |
| OsOSSeTe | $4.08 \times 10^{-11}$ | $5.11 \times 10^{-14}$ | $2.23 \times 10^{-13}$ | $3.40 \times 10^{-14}$ | $1.17 \times 10^{-13}$ | $1.35 \times 10^{-12}$ |



**Figure 5.** Electron chirality density ($\gamma^5$) calculated at HF (**a**), DFT PBE0 (**b**), and PBE (**c**) levels of theory.

Another model for testing the cooperative effects is to calculate PVED for stretched and contracted versions of the $Os_3(CO)_{12}$ cluster, where only the Os-Os distances change.

We may expect the decrease of geometric chirality parameter $\eta$ with the increase of the Os-Os distances. However, the calculated PVED values actually grow with increase of the Os-Os distances (Figure 6) for both HF and DFT PBE methods. This indicates that stronger interaction between Os atoms rather suppresses the electron chirality in the system.
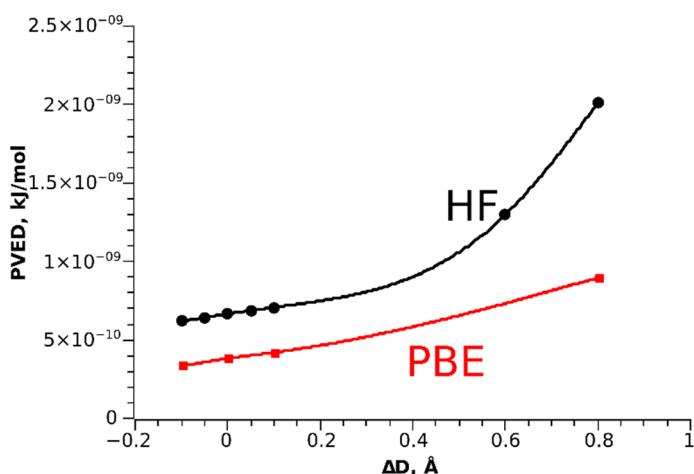


**Figure 6.** PVED as a function of Os-Os distance change, zero refers to the equilibrium Os-Os distance.

## 3. Materials and Methods

*Computational Details*

Geometry optimization of the $Os_3(CO)_{12}$ cluster with $D_3$ and $D_{3h}$ symmetries was performed in ADF2020 program [40,41] with all-electron Slater's type TZ2P basis set [42], TPSSh [43] density functional, and Grimme D4(EEQ) [44] dispersion corrections. The calculations were performed in the gas phase. In order to analyze the influence of the relativistic effects on the geometry of the cluster, the calculations were performed without relativistic approximation (NR), with scalar relativistic (SR), and with spin-orbit (SO) zero-order regular approximation (ZORA) [45,46]. To minimize the basis set superposition error (BSSE), the single point calculations at TPSSh + D4(EEQ) + SR/QZ4P level of theory were performed for the energy decomposition analysis (EDA) [47] and electron localization function calculations (ELF) [48,49]. ELF analysis was performed in the dgrid-4.6 program [50] on the discreet mesh with the step of 0.05 a.u.

The periodic calculation of the $Os_3(CO)_{12}$ cluster in the solid state were performed in the BAND2020 program [51,52] with SCAN density functional [53], all-electron TZP basis set, and SR ZORA approximation. The starting geometry for the periodic calculations was taken from the experimental XRD structural data [22].

Calculations of parity-violating energy difference (PVED) between left- and right-twisted structures of $Os_3(CO)_{12}$ in the gas phase were performed in Dirac-19 [32,54] with a fully relativistic four-component Dirac–Coulomb Hamiltonian. An all-electron double-zeta dyall.ae2z relativistic basis set [55], in combination with Hartree–Fock and various DFT methods, was used. To highlight the cooperative effect of three Os atoms, we compared the PVED for $Os_3(CO)_{12}$ with PVED for a hypothetical compound OsOSSeTe, where there was only one Os atom. The structure of OsOSSeTe in the gas phase was also optimized in ADF2020 at the TPSSh + D4(EEQ) + SR/QZ4P level of theory.

## 4. Conclusions

In our study, for the first time, the chirality of the $Os_3(CO)_{12}$ was investigated. With an account of relativistic effects, the twisted structure with the $D_3$ symmetry refers to the local minimum on potential energy surface, while the nonchiral $D_{3h}$ structure refers to the transition state with a single imaginary frequency. The chiral $D_3$ structure is, apparently, stabilized by the relativistic effects. Moreover, the EDA analysis of the interactions in $Os_3(CO)_{12}$ showed that $D_3$ structure has the stronger orbital interactions between $Os(CO)_4$ fragments.

The ELF topological analysis showed the unusual pattern of the basins. The trisynaptic basin in the center of Os triangle has no borders with any of the core basins, apparently, indicating the exchange between disynaptic V(Os, Os) basins.

We also estimated the PVED values for the $Os_3(CO)_{12}$ cluster. At present, the obtained values are the largest predicted, with the exception of the hypothetical $H_2Po_2$ system [31]. Moreover, the study of cooperative effects in PVED of $Os_3(CO)_{12}$ clusters showed that the stronger interaction between Os atoms rather reduces the electron chirality in the system. Knowing that, we may hope to construct in future some molecular system with even larger PVED.

**Supplementary Materials:** The following are available online, Table S1: Coordinates of the $Os_3(CO)_{12}$ cluster optimized with Non Relativistic (NR), Scalar Relativistic (SR) and Spin-Orbit (SO) approximations at TPSSh + D4(EEQ)/TZ2P level of theory, Figure S1: ELF basins for $Os_3CO_{12}$ clusters with $D_3$ (top) and $D_{3h}$ (bottom) symmetries, Figure S2: Critical points between V(Os, Os) and V(V(Os, Os)$_3$) basins.

**Author Contributions:** M.R.R.—quantum chemical studies of energy and structural parameters, conceptualization, and writing; I.V.M.—calculation of parity violation effects and writing; S.G.K. and Y.V.M.—discussion, writing, and editing. All authors have read and agreed to the published version of the manuscript.

**Institutional Review Board Statement:** Not applicable.

**Informed Consent Statement:** Not applicable.

**Data Availability Statement:** The data presented in this study are available in supplementary material.

**Conflicts of Interest:** There are no conflicts to declare.

**Sample Availability:** Samples of the compounds are not available from the authors.

# References

1. Kozlova, S.G.; Mirzaeva, I.V.; Ryzhikov, M.R. DABCO molecule in the $M_2(C_8H_4O_4)_2 \cdot C_6H_{12}N_2$ (M = Co, Ni, Cu, Zn) metal-organic frameworks. *Coord. Chem. Rev.* **2018**, *376*, 62–74. [CrossRef]
2. Kozlova, S.; Ryzhikov, M.; Pishchur, D.; Mirzaeva, I. Overview of Low-Temperature Heat Capacity Data for $Zn_2(C_8H_4O_4)_2$ $C_6H_{12}N_2$ and the Salam Hypothesis. *Symmetry* **2019**, *11*, 657. [CrossRef]
3. Puneet, P.; Singh, S.; Fujiki, M.; Nandan, B. Handed Mirror Symmetry Breaking at the Photo-Excited State of π-Conjugated Rotamers in Solutions. *Symmetry* **2021**, *13*, 272. [CrossRef]
4. Salam, A. The role of chirality in the origin of life. *J. Mol. Evol.* **1991**, *33*, 105–113. [CrossRef]
5. Berger, R. Parity-Violation Effects in Molecules. In *Relativistic Electronic Structure Theory, Part 2: Applications*; Schwerdtfeger, P., Ed.; Elsevier B.V.: Amsterdam, The Netherlands, 2004; pp. 188–288.
6. MacDermott, A.J.; Fu, T.; Nakatsuka, R.; Coleman, A.P.; Hyde, G.O. Parity-Violating Energy Shifts of Murchison L-Amino Acids are Consistent with an Electroweak Origin of Meteorite L-Enantiomeric Excesses Orig. *Life Evol. Biosph.* **2009**, *39*, 459–478. [CrossRef]
7. Schwerdtfeger, P. The Search for Parity Violation in Chiral Molecules. In *Computational Spectroscopy: Methods, Experiments and Applications*; Grunenberg, J., Ed.; Wiley-VCH Verlag GmbH & Co. KGaA: Weinheim, Germany, 2010; pp. 201–221.
8. Nizovtsev, A.S.; Ryzhikov, M.R.; Kozlova, S.G. Structural flexibility of DABCO. Ab initio and DFT benchmark study. *Chem. Phys. Lett.* **2017**, *667*, 87–90. [CrossRef]
9. Mirzaeva, I.V.; Kozlova, S.G. Parity violating energy difference for mirror conformers of DABCO linker between two $M^{2+}$ cations (M = Zn, Cd, and Hg). *J. Chem. Phys.* **2018**, *149*, 214302. [CrossRef] [PubMed]
10. Gabuda, S.P.; Kozlova, S.G. Abnormal difference between the mobilities of left- and right-twisted conformations of $C_6H_{12}N_2$ roto-symmetrical molecules at very low temperatures. *J. Chem. Phys.* **2015**, *142*, 234302. [CrossRef]
11. Mirzaeva, I.V.; Kozlova, S.G. Computational estimation of parity violation effects in a metal-organic framework containing DABCO. *Chem. Phys. Lett.* **2017**, *687*, 110–115. [CrossRef]
12. Vergeer, F.W.; Kleverlaan, C.J.; Matousek, P.; Towrie, M.; Stufkens, D.J.; Hartl, F. Redox Control of Light-Induced Charge Separation in a Transition Metal Cluster: Photochemistry of a Methyl Viologen-Substituted [$Os_3(CO)_{10}$(α-diimine)] Cluster. *Inorg. Chem.* **2005**, *44*, 1319–1331. [CrossRef] [PubMed]

13. Nijhoff, J.; Bakker, M.J.; Hartl, F.; Stufkens, D.J.; Fu; van Eldik, R. Photochemistry of the Triangular Clusters Os$_3$(CO)$_{10}$($\alpha$-diimine): Homolysis of an Os−Os Bond and Solvent-Dependent Formation of Biradicals and Zwitterions. *Inorg. Chem.* **1998**, *37*, 661–668. [CrossRef]

14. Adams, R.D.; Captain, B.; Zhu, L. A New Tris(diphenylstannylene)triosmium Carbonyl Cluster Complex and Its Reactions with Pt(PBu$^t_3$)$_2$ and Pt(PPh$_3$)$_4$. *Organometallics* **2006**, *25*, 2049–2054. [CrossRef]

15. Kuznetsov, B.N.; Kovalchuk, V.I.; Chesnokov, N.V.; Mikova, N.M.; Naimushina, L.V. Cluster carbonyls of Os, Fe and Fe-Rh on oxide supports: Synthesis and properties. *Macromol. Symp.* **1998**, *136*, 41–46. [CrossRef]

16. Bentsen, J.G.; Wrighton, M.S. Wavelength-, medium-, and temperature-dependent competition between photosubstitution and photofragmentation in triruthenium dodecacarbonyl and triiron dodecacarbonyl: Detection and characterization of coordinatively unsaturated trimetal undecacarbonyl complexes. *J. Am. Chem. Soc.* **1987**, *109*, 4530–4544.

17. Leadbeater, N.E. Control of the photochemistry of Ru$_3$(CO)$_{12}$ and Os$_3$(CO)$_{12}$ by variation of the solvent. *J. Organomet. Chem.* **1999**, *573*, 211–216. [CrossRef]

18. Schalk, O.; Josefsson, I.; Richter, R.; Prince, K.C.; Odelius, M.; Mucke, M. Ionization and photofragmentation of Ru$_3$(CO)$_{12}$ and Os$_3$(CO)$_{12}$. *J. Chem. Phys.* **2015**, *143*, 154305. [CrossRef]

19. Huggins, D.K.; Flitcroft, N.; Kaesz, H.D. Infrared Spectrum of Osmium Tetracarbonyl Trimer, Os$_3$(CO)$_{12}$; Assignment of CO and MC Stretching Absorptions. *Inorg. Chem.* **1965**, *4*, 166–169. [CrossRef]

20. Yan, S.; Seidel, M.T.; Zhang, Z.; Leong, W.K.; Tan, H.-S. Ultrafast vibrational relaxation dynamics of carbonyl stretching modes in Os$_3$(CO)$_{12}$. *J. Chem. Phys.* **2011**, *135*, 024501. [CrossRef]

21. Koridze, A.A.; Kizas, O.A.; Astakhova, N.M.; Petrovskii, P.V.; Grishin, Y.K. Internuclear exchange of carbonyl groups in Os$_3$(CO)$_{12}$: Coupling constants J($^{187}$Os–$^{13}$C) in trinuclear osmium carbonyls. *J. Chem. Soc. Chem. Commun.* **1981**, 853–855. [CrossRef]

22. Churchill, M.R.; DeBoer, B.G. Structural studies on polynuclear osmium carbonyl hydrides. 1. Crystal structures of the isomorphous species H$_2$Os$_3$(CO)$_{11}$ and Os$_3$(CO)$_{12}$. Role of an equatorial $\mu_2$-bridging hydride ligand in perturbing the arrangement of carbonyl ligands in a triangular cluster. *Inorg. Chem.* **1977**, *16*, 878–884.

23. Van der Maelen, J.F.; García-Granda, S.; Cabeza, J.A. Theoretical topological analysis of the electron density in a series of triosmium carbonyl clusters: [Os$_3$(CO)$_{12}$], [Os$_3$($\mu$-H)$_2$(CO)$_{10}$], [Os$_3$($\mu$-H)($\mu$-OH)(CO)$_{10}$], and [Os$_3$($\mu$-H)($\mu$-Cl)(CO)$_{10}$]. *Comput. Theor. Chem.* **2011**, *968*, 55–63. [CrossRef]

24. Hunstock, E.; Mealli, C.; Calhorda, M.J.; Reinhold, J. Molecular Structures of M$_2$(CO)$_9$ and M$_3$(CO)$_{12}$ (M = Fe, Ru, Os): New Theoretical Insights. *Inorg. Chem.* **1999**, *38*, 5053–5060. [CrossRef]

25. Li, Q.-S.; Xu, B.; Xie, Y.; King, R.B.; Schaefer, H.F. Unsaturated trinuclear osmium carbonyls: Comparison with their iron analogues. *Dalt. Trans.* **2007**, 4312–4322. [CrossRef]

26. Corey, E.R.; Dahl, L.F. The Molecular and Crystal Structure of Os$_3$(CO)$_{12}$. *Inorg. Chem.* **1962**, *1*, 521–526. [CrossRef]

27. Roberts, B.M.; Dzuba, V.A.; Flambaum, V.V. Parity and Time-Reversal Violation in Atomic Systems. *Annu. Rev. Nucl. Part. Sci.* **2015**, *65*, 63–86. [CrossRef]

28. Bast, R.; Koers, A.; Gomes, A.S.P.; Iliaš, M.; Visscher, L.; Schwerdtfeger, P.; Saue, T. Analysis of parity violation in chiral molecules. *Phys. Chem. Chem. Phys.* **2011**, *13*, 864–876. [CrossRef]

29. Schwerdtfeger, P.; Bast, R. Large Parity Violation Effects in the Vibrational Spectrum of Organometallic Compounds. *J. Am. Chem. Soc.* **2004**, *126*, 1652–1653. [CrossRef]

30. Faglioni, F.; Lazzeretti, P. Parity-violation effect on vibrational spectra. *Phys. Rev. A* **2003**, *67*, 032101. [CrossRef]

31. Berger, R.; van Wüllen, C. Density functional calculations of molecular parity-violating effects within the zeroth-order regular approximation. *J. Chem. Phys.* **2005**, *122*, 134316. [CrossRef]

32. Laerdahl, J.; Schwerdtfeger, P. Fully relativistic ab initio calculations of the energies of chiral molecules including parity-violating weak interactions. *Phys. Rev. A.* **1999**, *60*, 4439–4453. [CrossRef]

33. Rein, D.W.; Hegstrom, R.A.; Sandars, P.G.H. Parity non-conserving energy difference between mirror image molecules. *Phys. Lett. A* **1979**, *71*, 499–502. [CrossRef]

34. Harris, R.A.; Stodolsky, L. Quantum beats in optical activity and weak interactions. *Phys. Lett. B* **1978**, *78*, 313–317. [CrossRef]

35. Perdew, J.P.; Burke, K.; Ernzerhof, M. Generalized Gradient Approximation Made Simple. *Phys. Rev. Lett.* **1996**, *77*, 3865. [CrossRef] [PubMed]

36. Adamo, C.; Barone, V. Toward reliable density functional methods without adjustable parameters: The PBE0 model. *J. Chem. Phys.* **1999**, *110*, 6158–6169. [CrossRef]

37. Lee, C.; Yang, W.; Parr, R.G. Development of the Colle-Salvetti correlation-energy formula into a functional of the electron density. *Phys. Rev. B* **1988**, *37*, 785–789. [CrossRef] [PubMed]

38. Becke, A.D. Density-functional thermochemistry. III. The role of exact exchange. *J. Chem. Phys.* **1993**, *98*, 5648–5652. [CrossRef]

39. Yanai, T.; Tew, D.; Handy, N. A new hybrid exchange-correlation functional using the Coulomb-attenuating method (CAM-B3LYP). *Chem. Phys. Lett.* **2004**, *393*, 51–57. [CrossRef]

40. ADF, Version 2020.102, SCM, Theoretical Chemistry, Vrije Universiteit, Amsterdam, The Netherlands. Available online: https://www.scm.com/product/adf/ (accessed on 14 May 2021).

41. te Velde, G.; Bickelhaupt, F.M.; Baerends, E.J.; Fonseca Guerra, C.A.; van Gisbergen, S.J.; Snijders, J.G.; Ziegler, T. Chemistry with ADF. *J. Comput. Chem.* **2001**, *22*, 931–967. [CrossRef]

42. Van Lenthe, E.; Baerends, E.J. Optimized Slater-type basis sets for the elements 1–118. *J. Comput. Chem.* **2003**, *24*, 1142–1156. [CrossRef] [PubMed]

43. Tao, J.; Perdew, J.P.; Staroverov, V.N.; Scuseria, G.E. Climbing the Density Functional Ladder: Nonempirical Meta–Generalized Gradient Approximation Designed for Molecules and Solids. *Phys. Rev. Lett.* **2003**, *91*, 146401. [CrossRef] [PubMed]

44. Caldeweyher, E.; Ehlert, S.; Hansen, A.; Neugebauer, H.; Spicher, S.; Bannwarth, C.; Grimme, S. A generally applicable atomic-charge dependent London dispersion correction. *J. Chem. Phys.* **2019**, *150*, 154122. [CrossRef]

45. van Lenthe, E.; Ehlers, A.; Baerends, E.-J. Geometry optimizations in the zero order regular approximation for relativistic effects. *J. Chem. Phys.* **1999**, *110*, 8943–8953. [CrossRef]

46. van Lenthe, E.; Snijders, J.G.; Baerends, E.J. The zero–order regular approximation for relativistic effects: The effect of spin–orbit coupling in closed shell molecules. *J. Chem. Phys.* **1996**, *105*, 6505–6516. [CrossRef]

47. Ziegler, T.; Rauk, A. On the calculation of bonding energies by the Hartree Fock Slater method. *Theor. Chim. Acta.* **1977**, *46*, 1–10. [CrossRef]

48. Savin, A.; Jepsen, O.; Flad, J.; Andersen, O.K.; Preuss, H.; von Schnering, H.G. Electron Localization in Solid-State Structures of the Elements: The Diamond Structure. *Angew. Chem. Int. Ed. English.* **1992**, *31*, 187–188. [CrossRef]

49. Silvi, B.; Savin, A. Classification of chemical bonds based on topological analysis of electron localization functions. *Nature* **1994**, *371*, 683–686. [CrossRef]

50. Kohout, M. DGrid, Version 4.6, Radebeul, 2011. Available online: http://www.cpfs.mpg.de/~{}kohout/dgrid.html (accessed on 14 May 2021).

51. BAND, Version 2020.102, SCM, Theoretical Chemistry, Vrije Universiteit, Amsterdam, The Netherlands. Available online: https://www.scm.com/product/band_periodicdft/ (accessed on 14 May 2021).

52. te Velde, G.; Baerends, E.J. Precise density-functional method for periodic structures. *Phys. Rev. B* **1991**, *44*, 7888–7903. [CrossRef] [PubMed]

53. Sun, J.; Ruzsinszky, A.; Perdew, J.P. Strongly Constrained and Appropriately Normed Semilocal Density Functional. *Phys. Rev. Lett.* **2015**, *115*, 036402. [CrossRef]

54. Saue, T.; Bast, R.; Gomes, A.S.P.; Jensen, H.J.A.; Visscher, L.; Aucar, I.A.; Di Remigio, R.; Dyall, K.G.; Eliav, E.; Fasshauer, E.; et al. The DIRAC code for relativistic molecular calculations. *J. Chem. Phys.* **2020**, *152*, 204104. [CrossRef]

55. Dyall, K.G. Relativistic double-zeta, triple-zeta, and quadruple-zeta basis sets for the 6d elements Rf–Cn. *Theor. Chem. Acc.* **2011**, *129*, 603–613. [CrossRef]